ISSN 2072-5981
doi: 10.26907/mrsej

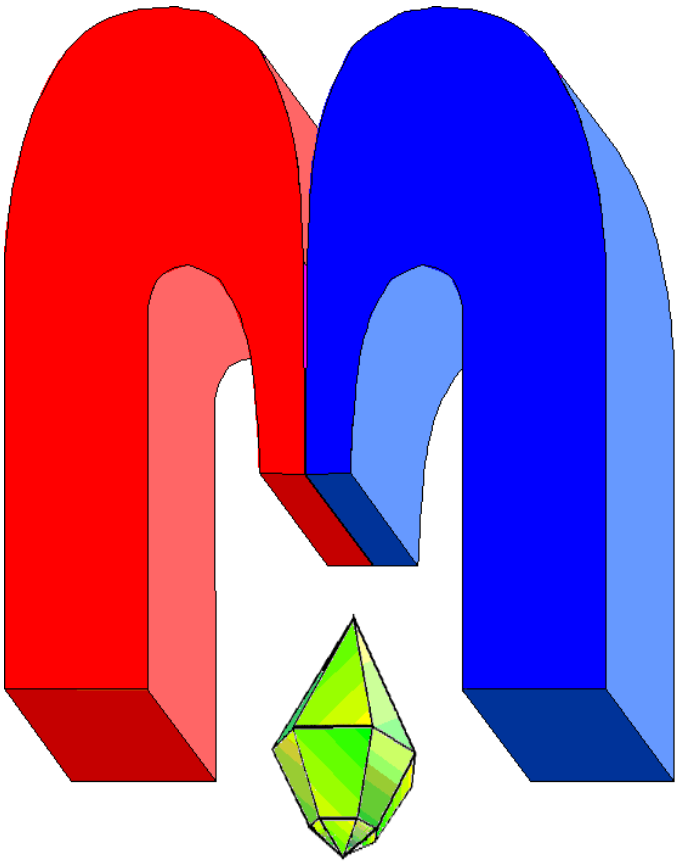

Magnetic Resonance in Solids

Electronic Journal

Volume 27
Issue 3
Article No ***25304***
1-12 pages
2025
doi: **10.26907/mrsej-25304**

http://mrsej.kpfu.ru
http://mrsej.elpub.ru

Established and published by Kazan University*
Endorsed by International Society of Magnetic Resonance (ISMAR)
Registered by Russian Federation Committee on Press (#015140), August 2, 1996
First Issue appeared on July 25, 1997

"***Magnetic Resonance in Solids. Electronic Journal***" (**MRS*ej***) is a peer-reviewed, all electronic journal, publishing articles which meet the highest standards of scientific quality in the field of basic research of a magnetic resonance in solids and related phenomena.

Indexed and abstracted by
Web of Science (ESCI, Clarivate Analytics, from 2015),White List (from 2023) *Scopus* (Elsevier, from 2012), *RusIndexSC* (*eLibrary*, from 2006), *Google Scholar*, *DOAJ*, *ROAD*, *CyberLeninka* (from 2006), *SCImago Journal & Country Rank*, etc.

* Address: "Magnetic Resonance in Solids. Electronic Journal", Kazan Federal University; Kremlevskaya str., 18; Kazan 420008, Russia

† In Kazan University the Electron Paramagnetic Resonance (EPR) was discovered by Zavoisky E.K. in 1944.

The early stages of the graphene oxide thermal decomposition explored by X– and W–band ESR and traditional methods

Sh. Galyaltdinov*, G.V. Mamin, A. Khannanov, M.R. Gafurov,
A. Kiiamov, D.A. Tayurskii, A.M. Dimiev*

Kazan Federal University, Kazan 420008, Russian

**E-mail: sgaljalt@kpfu.ru, AMDimiev@kpfu.ru*

(Received October 18, 2025; revised November 25, 2025;
accepted December 3, 2025; published December 11, 2025)

Thermal decomposition of graphene oxide (GO), often referred to as "thermal reduction" is broadly used to obtain so-called "thermally reduced GO". At the same time, chemical and structural transformations, accompanying this process remain largely unexplored. In this work, using the combination of electron spin resonance spectroscopy, thermogravimetry, IR spectroscopy, and X–ray powder diffraction, we investigate the early stages of the GO thermal decomposition, which occur in the 80°C–190°C temperature range. Massive decomposition of the oxygen-containing groups begins at ~ 130°C. At this temperature we observe formation of C-H bonds and a sharp increase in the content of paramagnetic centers. The highest content of the radicals 1.3×10^{18} spin/g is registered in the samples, annealed at 150°C. This is 3.5 times higher than that in original GO (3.8×10^{17} spin/g). At the same temperature we observe the loss of the interlayer registry in the material due to crumpling of the partially decomposed GO layers, and the C–H bonds are no longer observed. At 190°C, the content of the paramagnetic centers sharply decreases down to 1.0×10^{17} spin/g, being 3.8 times smaller than that in original GO. This suggests that electrons are largely delocalized due to the enlargement and percolation of graphenic domains, and/or dangling bonds, formed at 130–150°C largely recombine. Our new findings add critical details to understanding the fine chemical structure and chemistry of GO.

PACS: 71.70.Ch, 75.10.Dg, 76.30.Kg, 71.70.Ej.
Keywords: graphene oxide, paramagnetic centers, decomposition, electron spin resonance

1. Introduction

Graphene oxide (GO) is one of the most intensively studied materials in the last decade [1]. The presence of oxygen-containing functional groups on its surface opens up opportunities for its unlimited modification with various agents [2–4]. GO is widely used for applied purposes, such as the creation of catalysts [5,6], selective membranes [2,7], sorbents [8], and water purification [9,10]. Composite materials based on graphene, GO, and reduced GO (RGO), as well as conductive polymers, metal matrices, carbon-carbon matrices, and natural fibers, have potential applications in energy storage systems, clean energy storage devices, and wearable and portable electronics due to their excellent mechanical strength, conductivity, and exceptional thermal stability [11].

Due to their two-dimensional structure, graphene and graphene-based materials are highly attractive for spintronics and quantum computing. The discovery of spin resonance of conduction electrons and high charge mobility is a prerequisite for considering graphene for spintronics applications. To this end, electron spin resonance (ESR) and electrical resistance measurements were conducted on assemblies of GO and RGO flakes. These ESR measurements provided information on the defect density in the flakes [12].

The nature of the oxygen-containing groups in the GO structure is well determined by ^{13}C SS-NMR spectroscopy and IR spectroscopy [13]. The distance between GO sheets can be registered by X–ray powder diffractometry (XRD) [14], and the overall oxidation level and decomposi-

tion temperature range is determined by thermogravimetric analysis (TGA) [15]. Unlike the above-mentioned methods, ESR is not often used for GO characterization. Still, the spectra for neat GO and RGO have been reported [16, 17]. It was shown that typical GO possesses certain content of free radicals, while fully reduced, i.e. annealed GO contains no radicals due to delocalization of electrons, similar to that in graphene.

When heated, the oxygen-containing groups of GO undergo decomposition with the release of gaseous CO_2, CO, and H_2O, forming so-called thermally reduced graphene oxide [18]. The main decomposition temperature range for Hummers GO is 150–200°C, although higher temperatures are required to remove more stable groups [19]. Preheating below 100°C has been shown to result in no significant changes in the composition and structure of GO, but thermal treatment of GO at 150°C results in partial decomposition of oxygen functional groups without a significant increase in porosity [20].

The structure and chemistry of GO are still not fully understood. From these perspectives, the transformations in the GO structure, which occur at the early stages of thermal decomposition, have not been systematically studied. In this respect, one should mention the work of Lipatov et al. [21], where they studied the thermal decomposition of GO, by a combination of several methods such as mass-spectrometry, XPS, Raman spectroscopy, TEM, and electrical conductivity. An interesting observation the authors made is that between 135°C and 150°C the conductivity of GO increases sharply by five orders of magnitude, thus, material changes its character from non-conductive to conductive. Also, at 150°C they observe the highest rate of evolving gases CO_2, CO, and H_2O. Based on the observations, the authors conclude that at 150°C the size of graphenic domains increase to the level at which they start forming percolative paths.

The ESR spectra acquired during the thermal decomposition of GO shed some light on what occurs in the GO structure during the decomposition of oxygen-containing groups. ESR also provides quantitative information about the content of paramagnetic centers (PMC) in the material.

In this study, we studied the thermal decomposition of GO using ESR spectroscopy, supplemented with TGA, IR spectroscopy, and XRD. Namely, we subjected GO to partial thermal decomposition at temperatures in the 60–190°C range, and investigated the as-obtained products by the above-mentioned methods. The concentration of paramagnetic centers during the thermal decomposition of graphene oxide was determined.

2. Experimental

2.1. Materials.

Sulfuric acid (96%, Shchekinoazot LLC, Russia), potassium permanganate (99.5%, MCD Company, Russia), hydrogen peroxide (Tatkhimproduct JSC), hydrochloric acid (Tatkhimproduct JSC) were used without further purification.

2.2. Synthesis

Graphene oxide was obtained by the modified Hummers method [22]. Namely, graphite flakes (10 g) were dispersed in 96% sulfuric acid (625 mL) at room temperature and stirred with an overhead stirrer for 30 minutes. Then, 9 g $KMnO_4$ was added. The mixture became green due to formation of the MnO_3^+ cations. Additional portions of $KMnO_4$ (9 g) were added when the green color of MnO_3^+ was diminished, indicating that the previous portion of the oxidizing

agent was consumed. Eventually, 3.6 wt. equiv. of $KMnO_4$ were used in this synthesis. After full consumption of $KMnO_4$, the reaction was diluted with 1500 g of an ice/distilled water mixture and stirred for 1 hour. Next, 30% H_2O_2 solution was added dropwise (16 mL) to convert manganese by-products to soluble colorless Mn(II) ions. During this process, the color of the reaction mixture changed from pinkish to bright-yellow. Next, the reaction mixture was centrifuged 40 min at 5000 rpm to separate GO from the acid. For purification, the GO precipitate was redispersed in distilled water, stirred 60 min, and centrifuged 40 min at 5000 rpm to separate the purified GO from the washing water. This procedure constitutes one purification cycle. Four additional purification cycles were performed consecutively: the first time with distilled water, and three more times with HCl (4%). The GO precipitate after last washing was dried in air. After all these steps, 19.95 g of air-dried GO was obtained. Next, the samples of dried GO were annealed at different temperatures in nitrogen atmosphere for FTIR and for 1 hour in vacuum ($P < 10^{-4}$ mBar) for ESR measurements.

2.3. Characterization

- *The thermogravimetric analysis (TGA)* was performed with an STA 449 F5 Jupiter analyzer from Netzsch in Ar atmosphere in the range of 30–900°C.

- *The Fourier transform infrared (FTIR) spectra* of the studied solids were acquired with a Spectrum 400 FTIR spectrometer (PerkinElmer Inc.) with a Diamond KRS-5 attenuated total internal reflectance attachment (resolution was 0.5 cm^{-1}, 32 scans, wavelength range was 4000–500 cm^{-1}).

- *The powder X-ray diffractometry (XRD)* was performed with Bruker D8 Advance with Cu Kα irradiation ($\lambda = 1.5418$ Å) in the Bragg-Brentano geometry; the rate was 0.18°/min; the range of 2θ angle was from 5° to 35°; the step was 0.015°.

- *The X–band and W–band* ESR spectra with the microwave wave (MW) frequencies of about 9.6 and 94 GHz, correspondingly, were registered with Bruker ElexSys 580/680 ESR spectrometer at 25°C in continuous (CW) wave mode with a magnetic field modulation amplitude of 0.2 mT and modulation frequency of 100 kHz. The microwave power was 20 μW. The number of paramagnetic centers was measured following a standard method described in [23], by comparing the integrated intensity of the ESR lines of the measured sample and the integrated intensity of the $Cu(DETC)_2$ solution spectrum with Cu ions number of 7.2×10^{-9} mol. To probe nuclear spins, we use a standard Mims Electron-nuclear double resonance (ENDOR) pulse sequence to obtain changes in the stimulated spin echo (SSE) with sweeping of applied radiofrequency (RF): $\pi/2 - \tau - \pi/2 - \pi_{RF} - \pi/2 - \tau$–SSE [24]. The first two $\pi/2$ MW pulses invert the electron spin population; the third $\pi/2$ pulse generates SSE signal. Between the second and the third MW pulses, a radio frequency π_{RF} pulse with a duration of 16 μs is applied to invert the nuclear spin sublevels population, thereby inducing NMR transitions.

3. Results and Discussion

Figure 1 shows the results of thermogravimetric analysis for the original GO and the samples of GO annealed at different temperatures. Weight loss in the range of 30–140°C for the samples indicates the loss of sorbed water. It is seen that the initial GO contains the largest amount of water among the other samples. In the original GO, weight loss in this range is $\sim 10\%$, while in

all the other samples, weight loss does not exceed 6% of the original compound's weight. This suggests that after thermal treatment, GO sorbs less moisture from the atmosphere.

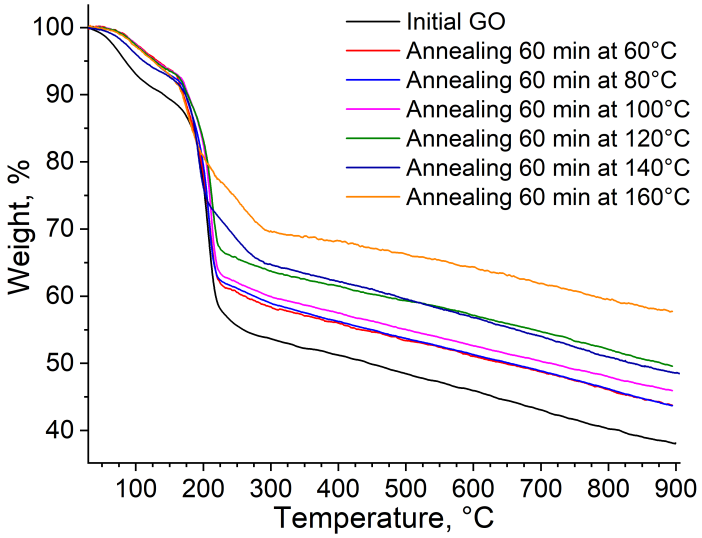

Figure 1. TGA curves of initial GO and samples of GO annealed at different temperatures for 60 min.

The weight loss in the range of 140–220°C is associated with decomposition of the main oxygen-containing groups, and the greater this weight loss is, the higher the overall oxidation level of the sample. The greatest weight loss of 33% is observed here for the original GO. The subjection of GO to thermal treatment results in the decrease of the weight loss in this temperature interval from 33% for original GO through 16% for the sample annealed at 160°C. The higher the annealing temperature of the sample, the lower the weight loss in this region.

In order to reveal what happens to the functional groups of GO during the thermal treatment, the FTIR spectra were recorded (Figure 2).

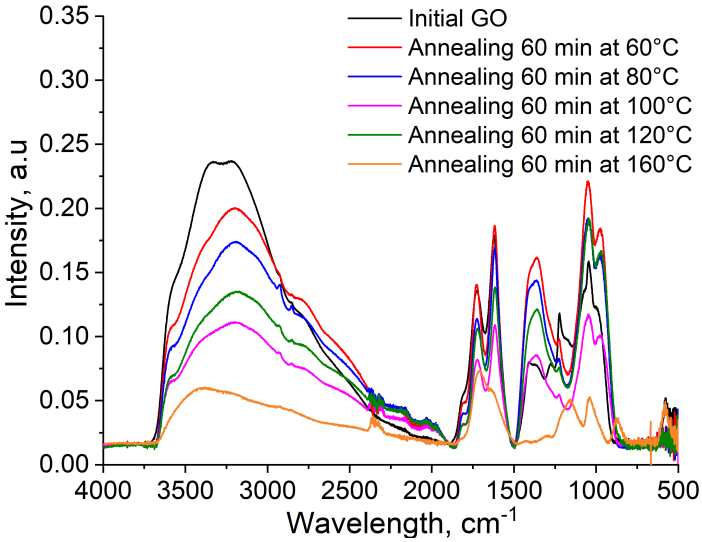

Figure 2. FTIR spectra of the initial GO and GO samples annealed at temperatures of 60, 80, 100, 120, 160°C for 60 minutes.

The IR spectrum shows that even after annealing at 160°C, the sample retains signals of associated hydrogen bonds in the 3700–2400 cm^{-1} region (Figure 2), clearly indicating that some

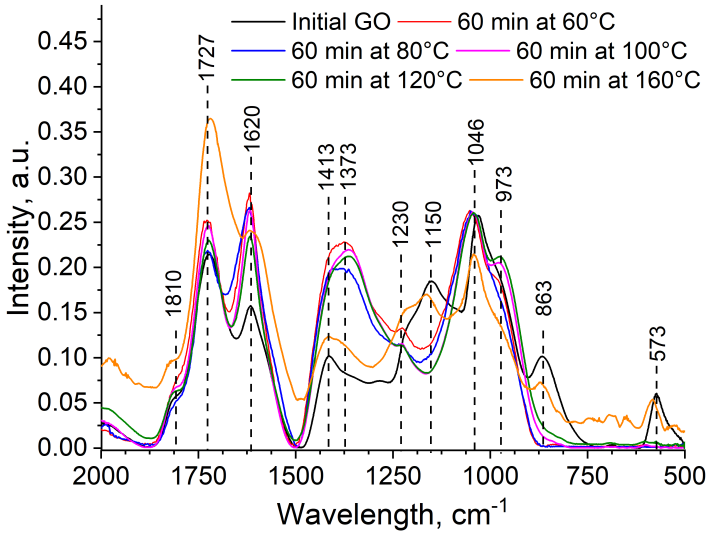

Figure 3. "Fingerprint region" of FTIR spectra of the initial GO and GO samples annealed at temperatures of 60, 80, 100, 120, 160°C for 60 minutes.

alcohol groups remain in the graphene oxide structure [13]. Also, the strong band at 1727 cm^{-1} suggests that the carboxyl groups are also in place (Figure 3). After annealing at 80, 100, and 120°C, the signals, associated with the stretch of C–H bonds at 2931 cm^{-1} and 2855 cm^{-1} are clearly visible. The maximum intensity of these signals is observed after annealing at 80°C, followed by a decrease in the intensity at 100°C. This behavior is associated with the rupture of C–C bonds and the formation of C–H bonds at the newly formed edges. At 160°C, these signals are no longer observed.

The most characteristic frequency range is the "fingerprint region". This region is the most informative for analyzing transformations of functional groups. Figure 3 shows FTIR spectra in the 2000–500 cm^{-1} range.

The signal at 1728 cm^{-1} is attributed to the stretching vibrations of C=O groups in carboxyl groups. This signal remains practically unchanged in all the thermally treated samples. The signals at 1413 cm^{-1} and 1228 cm^{-1} are caused, respectively, by asymmetric and symmetric vibrations of the S=O bonds of covalently bound sulfates [13]. The signals at 1046 cm^{-1} and 977 cm^{-1} are originate by alcohol and epoxy groups, respectively. The intensity of these groups largely remains for samples annealed at 80°C, 100°C, and 120°C, but significantly decreases for the sample, annealed at 160°C.

Figure 4 shows powder diffraction patterns of the original graphene oxide and GO samples annealed at different temperatures. A gradual decrease in the interplanar spacing between the GO sheets is observed, as the 2θ angle increases. For the sample, annealed at 160°C, the peak decreases in intensity, broadens and shifts toward larger 2θ angles. This observation is indicative of the loss of registry, i.e. amorphization due to crumpling of the decomposing GO sheets. The small peak at $\sim 12.4°$, is related to the presence of impurities in the initial graphite sample, used to prepare GO; this peak is present in all the acquired diffraction patterns. The same is true for a small peak at 25.0°. The low intensity halo in the 24–26° range is the newly forming (002) signal of RGO. However, its extremely low intensity suggests that formation of so-called "thermally reduced GO" is not yet achieved at this temperature.

Previously, the authors of works [25, 26] discovered that the ESR spectrum consists of two types of PMC, forming narrow and broad overlapping spectral components, which the authors

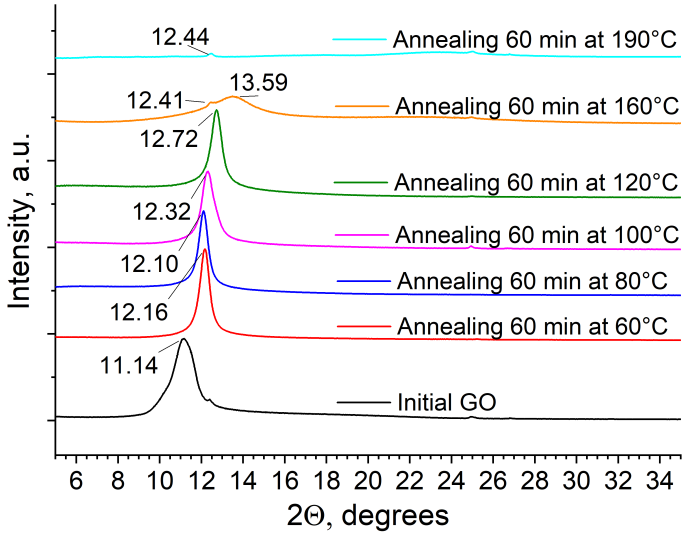

Figure 4. Powder diffraction patterns of graphene oxide and samples annealed at different temperatures.

designate as type 1 and type 2 radicals. For the type 1 radicals, the authors provide identical spectroscopic parameters $g = 2.0031$, while for the type 2 radicals, the g-factor varies from 2.0054 [26] to 2.002 [25]. To clarify the spectroscopic characteristics, we measured the ESR spectra of GO in the W–range (Figure 5A). Increasing the frequency increases the resolution in determining the g-factor, and the pulsed technique of recording the spectrum by the amplitude of the SSE allows one to separate components with different transverse relaxation times. The transverse relaxation time $T_2 = 210 \pm 2$ ns was measured for the ESR signal with $g = 2.0029$ and $T_2 = 1980 \pm 40$ ns for $g = 2.004$ (vertical lines on figure 5A). Longitudinal relaxation times are $134 \pm 5\,\mu$s and $187 \pm 30\,\mu$s, respectively. According to the technique described in [26], fast and slowly relaxing components of the spectrum were isolated from two ESR spectra recorded with different delays between the first and second MW pulses, shown in Figure 5 by the green and blue lines. Approximation (Figure 5, red lines) made it possible to determine the spectroscopic parameters of the obtained spectrum components (Table 1), and the complex shape of the line for free radicals with slow relaxation can only be described using two different components (crimson lines). The experimental spectra can be fitted by one type-1 component and two type-2 (2A and 2B) components (Table 1) with the corresponding parallel and perpendicular components of g-factors and linewidths. Significant changes in the intensity with thermal treatment were detected only for free radicals with narrower ESR spectra (first-type paramagnetic centers) (Figure 6), so only this type of PMC is discussed below.

Table 1. Spectroscopic parameters of the obtained spectrum (from Fig. 5) components

	Type of free radicals	$g_{\parallel}$	$g_{\perp}$	ΔH, mT
W–band	1	2.0029(2)	2.0044(2)	0.6(1)
	2 A	2.0040(4)		6.0(5)
	2 B	2.0004(2)	2.0028(2)	0.5(1)
X–band	1	2.0031(2)		0.27(1)
	2 A	2.0036(3)		0.32(1)
	2 B	2.0004(3)		0.51(2)

However, pulsed experiments do not allow one to determine the concentration of paramagnetic

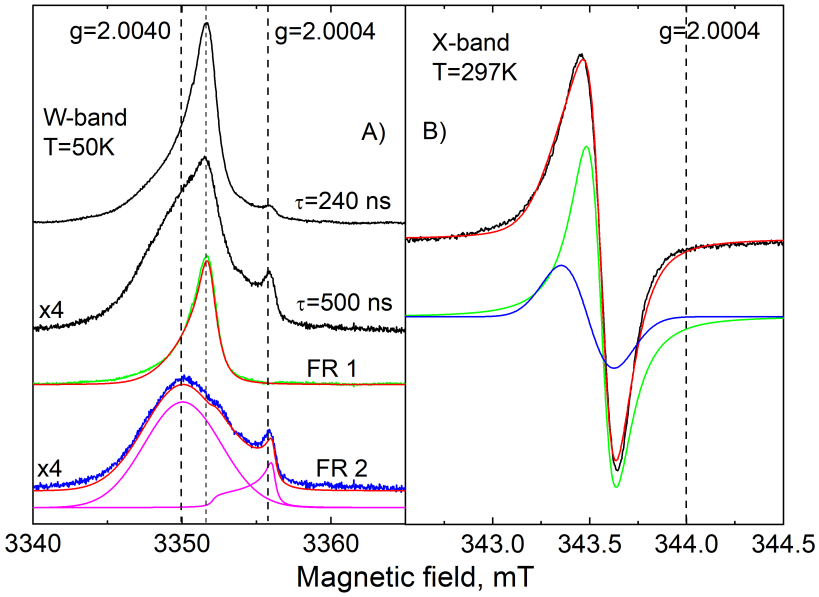

Figure 5. ESR spectrum of the GO sample after annealing at 50°C and its approximation: (A) W–band pulse regime, (B) X–band. Black lines are experiment, green lines are first-type paramagnetic center (FR1), blue lines are second-type paramagnetic center (FR2), red and magenta lines are fitting, FR are free radicals.

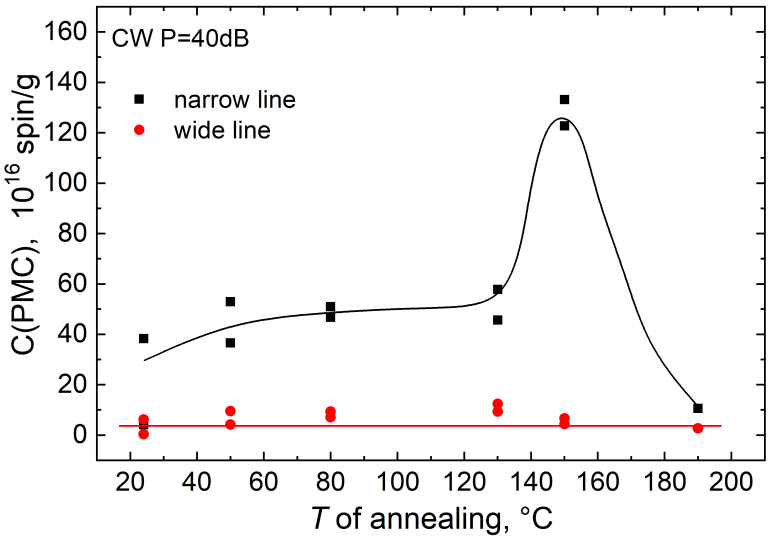

Figure 6. Dependence of the concentration of PMC on annealing temperature.

centers. Therefore, further measurements were performed in the X–band at room temperature in the spectrometer's CW mode. A typical ESR spectrum of GO is shown in Figure 5B and can be approximated with sufficient accuracy for determining the concentration by three components: a Lorentzian line and two Gaussian lines (see Table 1). As can be seen, experiments in W– and X–bands coincide with the W–band determined parameters with good accuracy. As can be seen from Table 1, the obtained parameters are in good agreement with those previously determined [16, 17, 25, 26].

Next, we acquired the ESR spectra for GO samples subjected to heating at different temperatures (Figure 7). It should be noted that the ESR spectrum of GO at room temperature is typical to those, reported for GO earlier [16, 17]. With increasing GO processing temperature,

the intensity of the ESR signal increases. This is indicative of formation of paramagnetic centers in GO due to the decomposition of GO functional groups with formation of "dangling" bonds.

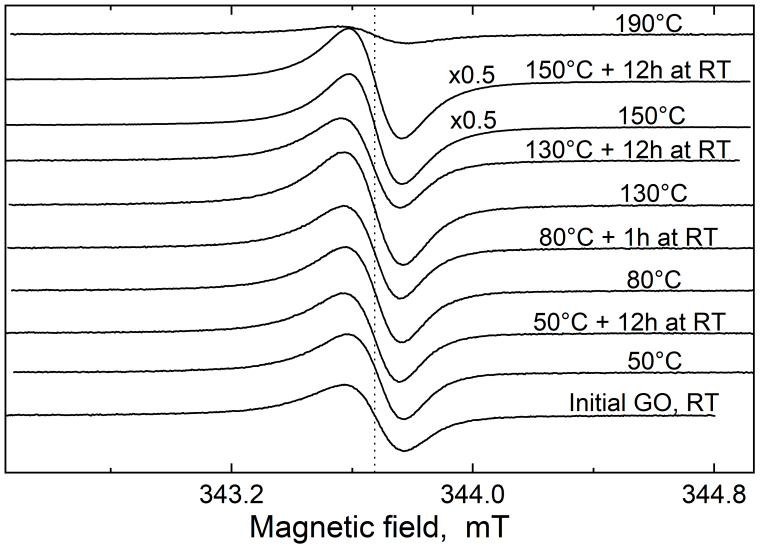

Figure 7. The ESR spectra of GO samples, thermally processed at different temperatures at X-band. The "+1h" and "+12h" captions show the time exposed at RT from the completion of the sample annealing to the start of ESR measurements.

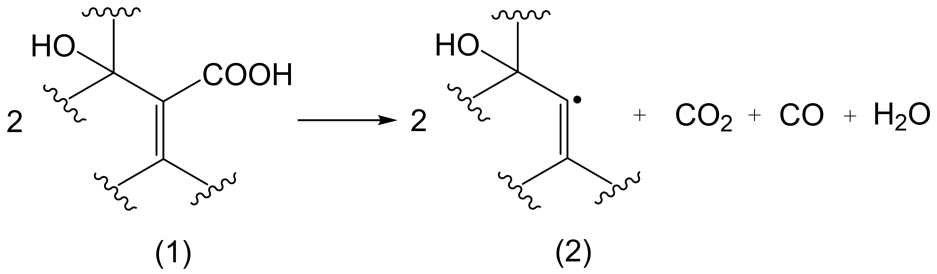

Figure 8. Possible scheme of formation of dangling bonds.

The most intense signal is observed at 150°C. At 190°C, the number of paramagnetic centers decreases significantly, and the signal drops sharply.

Table 2 presents the data on the concentration of first-type PMC (spin/g) in GO samples, annealed at different temperatures, calculated based on the spectra shown in Figure 7. The concentration of paramagnetic centers was calculated by double integration of the ESR spectra by intensity. T_1 and T_2 values were determined only for two samples by ESR pulse method.

The authors of the work [25] state that during decomposition of GO, stable radical species, such as semiquinones are formed. Formation of such structural fragments might be possible on the GO platform, but among the gaseous decomposition products are mainly CO_2, CO and H_2O with no radicals [18, 27].

At the initial stages of GO decomposition (50°C–150°C) the C–O and C–C bonds are ruptured, and the free radicals are formed. The highest content of the radicals is observed for the samples, annealed at 150°C; it was 3.5 times higher than that in the original GO. In Figure 8, we propose possible structural fragments with dangling bonds on the GO platform, and the way of

Table 2. Concentration and relaxation time of first-type free radicals in the samples of initial GO and GO annealed at different temperatures

Samples	C (PMC) (10^{17} spin/g)	T_2 (μs)	T_1 (μs)
Initial GO, RT	3.8 ± 2	0.576 ± 0.05	87 ± 5
GO annealed at 50°C	3.6 ± 2	–	
GO annealed at 50°C with keeping for 12 h at RT	5.2 ± 2	–	–
GO annealed at 80°C	4.6 ± 2	0.515 ± 0.05	60 ± 5
GO annealed at 80°C with keeping for 1 h at RT	5.0 ± 2	–	–
GO annealed at 130°C	5.7 ± 2	–	–
GO annealed at 130°C with keeping for 12 h at RT	4.5 ± 2	–	–
GO annealed at 150°C	12.2 ± 2	–	–
GO annealed at 150°C with keeping for 12 h at RT	13.3 ± 2	–	–
GO annealed at 190°C	1.0 ± 2	–	–

their formation. The gaseous decomposition products CO_2, CO and H_2O can be formed as result of the decarboxylation reaction, i.e. the loss of the carboxyl group. The reaction pathways leading to formation of carboxylic groups as results of thermal decomposition are numerous. Some of them are shown in the work [28]. Formation of the carboxyl groups always leads to formation of vacancy defects, thus carboxyl groups can exist only on the edge of a vacancy defect. In Figure 8, structure (1) transforms to structure (2), which bears unpaired electron, i.e. a dangling bond.

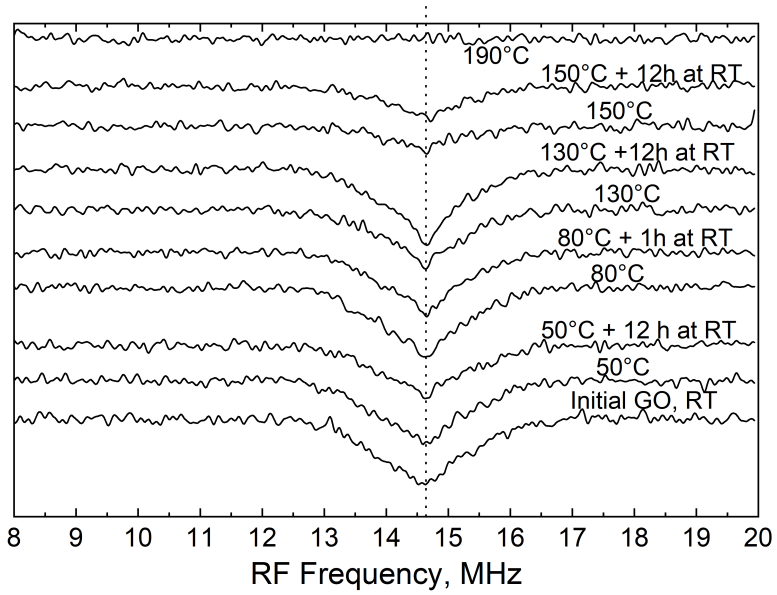

Figure 9. ENDOR spectra of GO and GO samples, annealed at different temperatures at X-band, $T = 297\,\mathrm{K}$, $B_0 = 343.8\,\mathrm{mT}$. The "+1h" and "+12h" captions show the time exposed at RT from the completion of the sample annealing to the start of ESR measurements.

After annealing at 190°C, the number of the paramagnetic centers decreases sharply (Figure 7, Table 2), and becomes even smaller than that in the parent GO. This occurs despite GO still retains appreciable content of oxygen groups, i.e. the material is far from attaining the graphite-like structure. We explain this observation by the fact that at 190°C the radicals of dangling bonds recombine.

Another possible explanation is delocalization of electrons due to the percolation of graphenic domains, as proposed by Lipatov et al. [21] based on the sharp increase in electrical conductivity. This transformation is indirectly observed in the ESR by a sharp increase in dielectric losses in the resonator. At this moment, we cannot state which process contributes more strongly to our observations.

Figure 9 shows the ENDOR spectra of the GO samples. The spectra were recorded at room temperature. ENDOR spectra reveal the interaction between the paramagnetic centers and the hydrogen nuclei in the sample, i.e. they show the content of both, and how close they are to each other. The line in the figure indicates the Larmor frequency for hydrogen nuclei. The narrower of the peak in the figure, the greater the distance between the paramagnetic center and the hydrogen nucleus from the OH groups and adsorbed water molecules in GO. At 190°C, the peak disappears due to the disappearance of hydrogen nuclei as a result of the nearly complete water desorption, and decomposition of the alcohol groups of GO. The narrowing of the peak for samples, annealed at 80°C and 130°C, suggests increasing the content of the radicals, and a decrease in the content of absorbed water and hydroxyl groups.

4. Conclusions

With the combination of several methods, we revealed the processes accompanying GO thermal decomposition at the beginning stages of this process. Using IR spectroscopy, it was shown that the thermal decomposition of GO is accompanied by the appearance of C–H bond stretching bands. These bonds are not present in the original GO, and might be formed only due to the rupture of C–O and C–C bonds. These bonds are no longer present in the sample, annealed at 160°C. Thermal decomposition of GO is accompanied by a decrease in the interplanar spacing between GO sheets due to the loss of water, followed by the broadening of the signal at 160°C, suggesting the loss of the interlayer registry due to crumpling of the decomposed GO layers. Using ESR, it was revealed that the thermal decomposition of GO leads to the rapid formation of paramagnetic centers at the newly formed defect sites. The highest content of the spins was observed for GO samples annealed at 150°C–160°C. At 190°C, the content of the local paramagnetic centers significantly decreases due to enlarging and percolating graphenic domains and/or recombination of spins. The thermal decomposition process is not fully reproducible in terms of the exact quantity of paramagnetic centers, formed at certain temperatures. Our new findings add critical details to understanding the fine chemical structure and chemistry of GO.

Acknowledgments

This work was performed with support of the funds allocated by Kazan Federal University for the project “Materials for green energy and sustainablity”.

References

1. Dimiev A. M., Eigler S., *Graphene Oxide: Fundamentals and Applications* (Cambridge International Science Publishing, 2016).

2. Vishwakarma R. K., Narayanam P. K., Umamaheswari R., Polaki S. R., *J. Water Process Eng* **51**, 103329 (2023).

3. Lin H., Li Y., Zhu J., *J. Memb. Sci.* **598**, 117789 (2020).

4. Ma H. L., Zhang H. B., Hu Q. H., Li W. J., Jiang Z. G., Yu Z., Dasari A., *ACS Appl. Mater. Interfaces* **4**, 1948 (2012).

5. Svalova A., Brusko V., Sultanova E., Kirsanova M., Khamidullin T., Vakhitov I., Dimiev A. M., *Appl. Surf. Sci.* **565**, 150503 (2021).

6. Song P., Feng J. J., X S., Zhong, Huang S. S., Chen J. R., Wang A. J., *RSC Adv.* **5**, 35551 (2015).

7. Galyaltdinov S., Safina G., Kiiamov A., Dimiev A., *Langmuir* **40**, 17667 (2024).

8. de Assis L. K., Damasceno B. S., Carvalho M. N., Oliveira E. H. C., Ghislandi M. G., *Environ. Technol.* **41**, 2360 (2020).

9. Yang J., Shojaei S., Shojaei S., *Npj Clean Water* **5**, 1 (2022).

10. Jin Q. Q., Zhu X. H., Xing X. Y., Ren T. Z., *Adsorpt. Sci. Technol.* **30**, 437 (2012).

11. Razaq A., Bibi F., Zheng X., Papadakis R., Hassan S., Jafri M., *Materials* **15**, 1012 (2022).

12. Airić L., Sienkiewicz A., Gaál R., Jaćimović J., Vĝju C., Magrez A., Forró L., *Phys. Rev. B* **86**, 1 (2012).

13. Brusko V., Khannanov A., Rakhmatullin A., Dimiev A., *Carbon* **229**, 119507 (2024).

14. Storm M. M., Johnsen R. E., Norby P., *J. Solid State Chem.* **240**, 49 (2016).

15. Gutiérrez-Portocarrero S., Roquero P., Becerril-González M., Zúniga-Franco D., *Diam. Relat. Mater.* **92**, 219 (2019).

16. Augustyniak-Jablokow M. A., Tadyszak K., Strzelczyk R., Fedaruk R., Carmieli R., *Carbon* **152**, 98 (2019).

17. Kempi'nski M., Florczak P., Jurga S., Śliwińska-Bartkowiak M., Kempiński W., *Appl. Phys. Lett.* **111**, 084102 (2017).

18. Mcallister M. J., Li J., Adamson D. H., Schniepp H. C., Abdala A. A., Liu J., Herrera-Alonso M., Milius D. L., Car R., Prudḥomme R. K., Aksay I. A., *Chem. Mater.* **19**, 4396 (2007).

19. Menezes I. R. S., Araújo N. R. S., Araújo B. C. R., Sakai T., Lago R. M., Sebastiao R. C. O., *Thermochim. Acta* **721**, 084102 (2023).

20. Menezes I. R. S., Sakai T., Hattori Y., Kaneko K., *Chem. Phys. Lett.* **807**, 140091 (2022).

21. Lipatov A., Guinel M. J.-F., Muratov D. S., Vanyushin V. O., Wilson P. M., Kolmakov A., Sinitskii A., *Appl. Phys. Lett.* **112**, 053103 (2018).

22. Dimiev A. M., Shukhina K., Khannanov A., *Carbon* **166**, 1 (2020).

23. Bertrand P., *Electron Paramagnetic Resonance Spectroscopy* (Springer, Berlin/Heidelberg, Germany, 2022).

24. Mims W. B., *Proc. R. Soc. London. Ser. A. Math. Phys. Sci.* **283**, 452 (1965).

25. Wang B., Fielding A. J., Dryfe R. A. W., *J. Phys. Chem. C* **123**, 22556 (2019).

26. Panich A., Shames A., Sergeev N., *Appl. Magn. Reson.* **44**, 107 (2013).

27. Jankovský O., Lojka M., Nováúek M., Luxa J., Sedmidubský D., Pumera M., Kosinac J., Sofer Z., *Green Chem.* **18**, 6618 (2016).

28. Dimiev A. M., Polson T. A., *Carbon* **93**, 544 (2015).